MODELING AND SIMULATION OF BLADDER POWER PUMP DRIVEN BY EXTERNAL ELECTROMAGNET

X. Li *

School of Electromechanical Engineering
Guangdong University of Technology
Guangzhou 510006, P. R. China

T. Guan

Guangzhou General Hospital of Guangzhou Military Command
Guangzhou 510010, P. R. China

W.-J. Huang **C.-H. Liang**

School of Electromechanical Engineering
Guangdong University of Technology
Guangzhou 510006, P. R. China

ABSTRACT

The clinical urination assist measures are usually taken to overcome the neurogenic bladder difficult to cure, but easily cause patients bladder stones, urinary system infection and other complications. To solve the problem of the urination assist of neurogenic bladder, a bladder power pump (BPP) driven by external electromagnet was proposed in this study according to the structure and micturition mechanism of human urinary bladder. The mathematic models of the BPP were established based on the theories of electromagnetics and fluid dynamics. A simulated experiment system with a bladder physical model for simulating human urinary system was designed according to the similarity criterion of fluid dynamincs. The micturition performance of the BPP was investigated by simulation and experiment. The results showed that the intravesical pressure and urine flow rate of the bladder physical model can be controlled by adjusting electromagnet exciting current. The micturition performance of the BPP is basically accordant with that of human urinary bladder detrusor. The established mathematic models are simple and practicable, which can provide the theoretical guidance for the performance analysis and structural optimization design of the BPP.

Keywords: Bladder power pump, Electromagnetic drive, Mathematic model, Simulation.

1. INTRODUCTION

The neurogenic bladder is a term applied to a malfunctioning urinary bladder due to neurologic dysfunction or insult emanating from internal or external trauma, disease, or injury. The symptoms of neurogenic bladder, such as incontinence, dysuria and urine retention, not only bring patients great pain and life troubles, but also cause urinary system infection, bladder stones, hydronephrosis and renal failures, even endanger their life [1].

The treatment of neurogenic bladder is one of the acknowledged difficult problems in the world. A number of scholars were engaged in the researches of the therapy and urination assist measures of neurogenic bladder [2-8]. Wiart *et al.* [9] perfused capsaicin into patient's urinary bladder in order to alleviate the symptoms of neurogenic bladder. But, the side effect from the drug was the presence of blood in the urine. Robin *et al.* [10] developed an electrical stimulation device that induces urinary bladder micturating by stimulating sacrum nerve. The curative effect of the device is still under experiment research. Xiao *et al*. [11,12] established an artificial somatic-autonomic reflex arc of inducing urinary bladder micturating by using paraplegic leg's waste nerve. The shortcoming is that the patients with healthy legs may be unwilling to accept such treatment. Operation therapy is only suitable for few symptoms, and easily brings about some complications [13]. Exerting pressure upon patient's belly cannot empty the urine in urinary bladder, thus cause bladder stones, and urinary system infection. Intubating urethra or conducting fistula into urinary bladder cause patient a great deal of pain. Kazuo *et al.* [14,15] proposed an urination assist system that pushes patient's urinary bladder by using shape memory alloy (SMA) springs. Peltier elements are used for controlling the temperature of SMA springs. The disadvantages are that the architecture of the system is complicated, and the electrical wires are needed for passing through patient's abdominal wall. Up to now, the effective clinical urination assist measures have not yet been found.

* Corresponding author (lixiao@gdut.edu.cn)

DOI : 10.1017/jmech.2012.106
Copyright © 2012 The Society of Theoretical and Applied Mechanics, R.O.C.
https://doi.org/10.1017/jmech.2012.106 Published online by Cambridge University Press

Aiming at the problem of the urination assist of neurogenic bladder, we proposed a new method to assist neurogenic bladder micturating with electromagnetic power device [16]. In this paper, a bladder power pump (BPP) driven by external electromagnet is presented, the working principle and features of the BPP are explained, the mathematic models of the BPP are established, and the micturition performance of the BPP is investigated by simulation and experiment, as well as the effectiveness of the BPP is evaluated.

2. BlADDER POWER PUMP

2.1 Micturition Mechanism of Urinary Bladder

As shown in Fig. 1, urinary bladder is a vesica of storing urine, which is connected with ureters and urethra respectively. The ureters convey the urine from kidney to urinary bladder by means of the peristalsis of ureter sphincters. When the urinary bladder is filled with the urine to a certain extent, the nerves to urinary bladder control urinary bladder detrusor to contract, and also control urethra sphincter to relax. As a result, the ureters in urinary bladder wall are pressed, the ureter orifices are closed, and the reflux of urine is prohibited; the urethra orifice is opened and the urine is expelled from the urinary bladder. After emptying, the urinary bladder resumes the storing of urine [17].

2.2 Working Princple of Bladder Power Pump

According to the structure and micturition mechanism of urinary bladder, a BPP driven by external electromagnet was proposed in this study, as shown in Fig. 2. It is composed of magnetic mover, stator and external electromagnet. The dish-shape stator that is made from nonmagnetic material is fastened to pubis. The external electromagnet that consists of direct-current coil and electromagnetic core is placed on abdominal wall. The magnetic mover is composed of silicon rubber membrane and some permanent magnets (PMs) distributed in the membrane. The ends of the membrane are fastened to the stator, which forms an alterable working chamber of covering urinary bladder. A rubber ring embedded in the membrane wraps the urethra, which forms a switch valve of urethra. The external electromagnet together with the magnetic mover forms an electromagnetic drive.

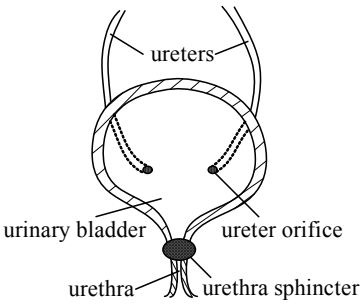


Fig. 1 Sketch map of urinary bladder

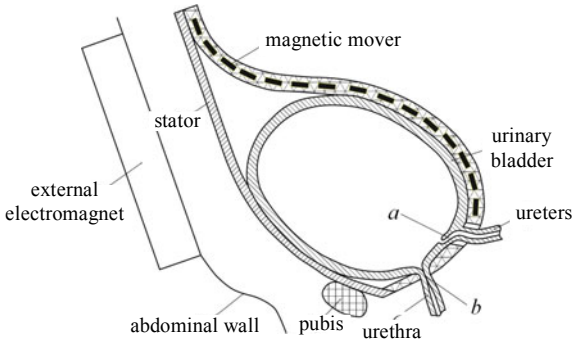


Fig. 2 Working principle map of BPP

The working principle of the BPP is described as follows:

In the urine storage stage, the external electromagnet is in the power-off state. The electromagnetic field is not founded. The magnetic mover keeps a relaxed state because no electromagnetic driving force is acting on it. Since the urinary bladder is not pressed by the magnetic mover, the ureter orifices (a) are opened. As the rubber ring wraping the urethra maintains the contractile state, the urethra orifice (b) is closed. Meanwhile, the urine from kidney is conveyed to the urinary bladder due to the peristalsis of ureter sphincters. With the accumulation of the urine, the urinary bladder expands and actuates the magnetic mover going up gradually.

In the micturition stage, the external electromagnet is in the energized state. The electromagnetic field is founded. The PMs of the magnetic mover are respectively pulled to the stator by the electromagnetic driving force. The membrane of the magnetic mover is ceaselessly tensed. As a result, the urinary bladder is pressed by the magnetic mover, the ureter orifices (a) are closed, and the urethra orifice (b) is opened. The urine is continuously discharged out from the urethra.

Thus it can be seen, the proposed pump has following features:

- The urinary bladder, urethra and ureters are not incised for installing the parts of apparatus, thus, the dissection structure of urinary system is not damaged.
- The magnetic mover and stator are not touched with urine, the infection of urinary system and subsequent complication are avoided.
- The working chamber formed by both magnetic mover and stator need not be sealed, no abrasion and heat occur.
- The flexible rubber is adopted to open and close the ureters and urethra orifices, no mechanical trauma is caused.
- The ureters and urethra orifices are sealed by their respective inner walls to prevent the leakage and reflux of the urine.
- The PMs of magnetic mover are wrapped by rubber membrane, they will not rust; the stator is made from the nonmagnetic materials, it is consistent with human physiological tissues.

https://doi.org/10.1017/jmech.2012.106 Published online by Cambridge University Press

3. MATHEMATIC MODELS

In the following modeling, we assume that the displacement current, the temperature effects on the conductance and permeability, and the elasticities of rubber membrane and urinary bladder are neglected respectively, as well as the magnetization of PM are parallel.

3.1 Mathematic Model of Electromagnetic Drive

The sketch map of the structure of electromagnetic drive is shown in Fig. 3. For the convenience of modeling, the local coordinate system *xyz* is established. The direction of remnant magnetization intensity of PM is parallel to *x*-axis, the normal of the maximum side surface of PM is parallel to *z*-axis, and symbol θ denotes the angle of PM relative to the plane of *X*-*Y*.

There is a magnetization surface-electric-current on the side surfaces parallel to the direction of remnant magnetization intensity of PM, the density of the magnetization surface-electric-current is described as

$$\boldsymbol{J}_m = \frac{\boldsymbol{B}_r}{\mu_0 \mu_{rec}} \tag{1}$$

where, $\boldsymbol{B}_r$ is the remnant magnetic induction intensity of PM; μ_0 is the permeability of vacuum; μ_{rec} is relative recoil permeability.

According to Biot-Savart law [18], the magnetic vector potential of a point $P(x, y, z)$ in the electromagnetic field that is established by the exciting current I of the direct-current coil of electromagnet is expressed as

$$\boldsymbol{A}_w = \frac{\mu_0 I}{4\pi}\int_l \frac{\mathrm{d}\, l}{R} \tag{2}$$

where, R is the distance from differential element $\mathrm{d}\boldsymbol{l}$ to the point P; l is the leads length of direct-current coil.

The magnetic vector potential of the point $P(x, y, z)$ that is established by electromagnet core is expressed as

$$\boldsymbol{A}_c = \frac{\mu_0}{4\pi}\int_{V_c} \frac{\boldsymbol{J}_{cv}}{R_c}\mathrm{d}V_c + \frac{\mu_0}{4\pi}\int_{S_c} \frac{\boldsymbol{J}_{cs}}{R_c}\mathrm{d}S_c \tag{3}$$

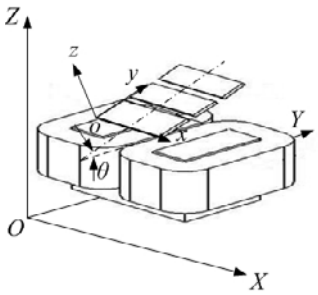


Fig. 3 Sketch map of the structure of electromagnetic drive

where, $\boldsymbol{J}_{cv}$ is the density of magnetization body-electric-current in electromagnet core; $\boldsymbol{J}_{cs}$ is the density of magnetization surface-electric-current on electromagnet core; V_c is the volume of electromagnet core; S_c is the surface area of electromagnet core; R_c is the distance from electromagnet core to the point P.

The magnetic vector potential of the point $P(x, y, z)$ that is established by PM is expressed as

$$\boldsymbol{A}_m = \frac{\mu_0}{4\pi}\int_{s_m} \frac{\boldsymbol{J}_m}{R_m}\mathrm{d}S_m \tag{4}$$

where, S_m is the surface area of PM; R_m is the distance from PM to the point P.

Therefore, the magnetic vector potential of the point $P(x, y, z)$ that is established by the electromagnetic drive is expressed as

$$\boldsymbol{A} = \boldsymbol{A}_w + \boldsymbol{A}_c + \boldsymbol{A}_m \tag{5}$$

Since the divergence of magnetic induction intensity $\boldsymbol{B}$ is always zero, the curl of $\boldsymbol{B}$ can be expressed as $\boldsymbol{B} = \nabla \times \boldsymbol{A}$. Thus, the magnetic induction intensity of the point $P(x, y, z)$ is written as

$$\boldsymbol{B} = \nabla \times (\boldsymbol{A}_w + \boldsymbol{A}_c + \boldsymbol{A}_m) \tag{6}$$

The diagram of the force analysis of the differential elements of the magnetization surface-electric-current on PM is shown in Fig. 4. The dashed lines represent magnetic field lines.

The magnetic induction intensities in *x*-axis direction at point P_1 and P_2 are respectively

$$B_x(x_1, y_1, z_1) = B(x_1, y_1, z_1)\cos\theta_1 \tag{7}$$

$$\begin{aligned} B_x(x_2, y_2, z_2) &= B(x_1, y_1, z_2)\cos\theta_2 \\ &= B_x(x_1, y_1, z_1) + \int_{z_1}^{z_2} \frac{\partial B_x(x_1, y_1, z)}{\partial z}\mathrm{d}z \end{aligned} \tag{8}$$

According to the formula of Lorentz force, *i.e.* $\mathrm{d}\boldsymbol{F} = I\mathrm{d}\boldsymbol{l} \times \boldsymbol{B} = \boldsymbol{J}_m \times \boldsymbol{B}\mathrm{d}S$, the magnetic forces acting on the differential elements of the magnetization surface-electric-current can be expressed as

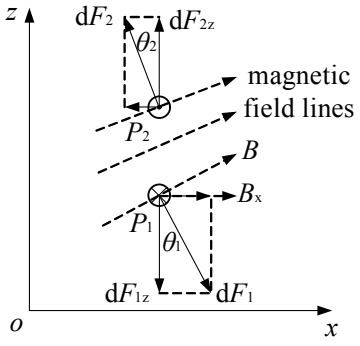


Fig. 4 Diagram of force analysis of differential elements of magnetization surface-electric-current on PM

https://doi.org/10.1017/jmech.2012.106 Published online by Cambridge University Press

$$dF_{1z} = -J_m B_x(x_1, y_1, z_1)dxdy \tag{9}$$

$$dF_{2z} = J_m B_x(x_2, y_2, z_2)\,dx\,dy \tag{10}$$

$$dF_{12z} = dF_{1z} + dF_{2z} = J_m\left(\int_{z_1}^{z_2} \frac{\partial B_x(x_1, y_1, z)}{\partial z} dz\right) dx\,dy \tag{11}$$

where, dF_{1z} and dF_{2z} denote the magnetic forces acting on the differential element of the magnetization surface-electric-current in z-axis direction at point P_1 and P_2 respectively, dF_{12z} is the sum of dF_{1z} and dF_{2z}.

From Eqs. (1) and (11), the magnetic force acting on PM in z-axis direction can be educed as

$$F_z = \frac{B_r}{\mu_0 \mu_{rec}} \int_{x_0}^{x_0+a} \int_{y_0}^{y_0+b} \int_{z_0}^{z_0+h} \frac{\partial B_x}{\partial z} dz\,dy\,dx \tag{12}$$

where, x_0, y_0 and z_0 are the initial coordinates of PM in the local coordinate system xyz; a, b and h are the lengths of PM in x, y and z-axis direction respectively.

So, the magnetic force acting on PM in y-axis direction can be educed as

$$F_y = \frac{B_r}{\mu_0 \mu_{rec}} \int_{x_0}^{x_0+a} \int_{z_0}^{z_0+h} \int_{y_0}^{y_0+b} \frac{\partial B_x}{\partial y} dy\,dz\,dx \tag{13}$$

The diagram of the force analysis of PM is shown in Fig. 5.

The magnetic force acting on PM in Z-axis direction can be expressed as

$$F_Z = F_z \cos\theta + F_y \sin\theta \tag{14}$$

By substituting Eqs. (12) and (13) into Eq. (14), the magnetic force can be described as

$$F_Z = \frac{B_r}{\mu_0 \mu_{rec}} \int_{x_0}^{x_0+a} \int_{y_0}^{y_0+b} \int_{z_0}^{z_0+h} \frac{\partial B_x}{\partial z} dz\,dy\,dx \cos\theta + \frac{B_r}{\mu_0 \mu_{rec}} \int_{x_0}^{x_0+a} \int_{z_0}^{z_0+h} \int_{y_0}^{y_0+b} \frac{\partial B_x}{\partial y} dy\,dz\,dx \sin\theta \tag{15}$$

The change rates of B_x in y and z-axis direction can be regarded as constant owing to the small PM. Therefore, Eq. (15) becomes

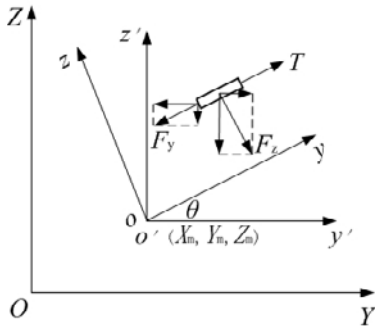


Fig. 5 Diagram of force analysis of PM

$$F_Z \approx \frac{B_r V}{\mu_0 \mu_{rec}} \left(\frac{\partial B_x}{\partial z}\cos\theta + \frac{\partial B_x}{\partial y}\sin\theta\right) \tag{16}$$

where, V is the volume of PM, $V = abh$.

Since $\frac{\partial B_x}{\partial y} = \frac{\partial B_x}{\partial z}\frac{\partial z}{\partial y} \approx \frac{\partial B_x}{\partial z}\frac{h}{b}$, Eq. (16) becomes

$$F_Z \approx \frac{B_r V}{\mu_0 \mu_{rec}} \frac{\partial B_x}{\partial z}\left(\cos\theta + \frac{h}{b}\sin\theta\right) \tag{17}$$

The transform relationships of the coordinate systems are respectively

$$\begin{cases} z = z'\cos\theta - y'\sin\theta \\ y = z'\sin\theta + y'\cos\theta \\ x = x' \end{cases} \tag{18}$$

$$\begin{cases} z' = Z - Z_m \\ y' = Y - Y_m \\ x' = X - X_m \end{cases} \tag{19}$$

By substituting Eqs. (18) and (19) into Eq. (17), the magnetic force is written as

$$F_Z \approx \frac{B_r V}{\mu_0 \mu_{rec}} \frac{\partial B_X}{\partial Z}\left(1 + \frac{h}{b}\tan\theta\right) \tag{20}$$

The magnetic induction intensity is proportional to electric current and the permeability of vacuum, and inversely proportional to the square of air gap. So, Eq. (20) becomes

$$F_Z = -K\frac{B_r VNI}{\mu_{rec}\delta^2}(1 + \chi\tan\theta) \tag{21}$$

where, δ is the air gap between electromagnet and PM; N is the turns of coil ; χ is the structure coefficient of PM; K is a flux leakage coefficient; "-" means F_Z is in $-Z$-axis direction

From Eq. (21), the electromagnetic driving force acting on the magnetic mover is educed

$$F = -K\frac{B_r VNI}{\mu_{rec}}\sum_{i=1}^{n}\frac{1}{\delta_i^2}(1 + \chi\tan\theta_i) \tag{22}$$

where, δ_i is the air gap between the ith PM and the electromagnet; θ_i is the angle of the ith PM relative to the plane of X-Y; n is the number of PMs.

3.2 Mathematic Model of Urinary Bladder

Considering the convenience of modeling, we perform a force analysis of magnetic mover. The diagram of the force analysis of magnetic mover is shown in Fig. 6.

The force equations of magnetic mover are described as

$$R\cos\gamma - \sum_{i=1}^{n}|F_{Zi}| - T_1\cos\alpha - T_2\cos\beta = 0 \tag{23}$$

$$R\sin\gamma + T_2\sin\beta - T_1\sin\alpha = 0 \tag{24}$$

https://doi.org/10.1017/jmech.2012.106 Published online by Cambridge University Press

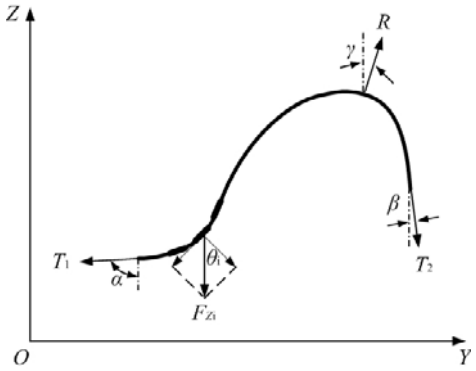


Fig. 6 Diagram of force analysis of magnetic mover

where, R denotes the support force acting on magnetic mover from urinary bladder; T_1 and T_2 represent the tensile forces acting on the ends of magnetic mover from stator; α is the angle between T_1 and –Z-axis, β is the angle between T_2 and –Z-axis, and γ is the angle between R and Z-axis.

The tensile forces equation is expressed as

$$T_2 - \sum_{i=1}^{n} \left| F_{Zi} \right| \sin\theta_i - T_1 = 0 \tag{25}$$

A differential element dA is chosen on the contact surface of magnetic mover with urinary bladder. Then, the integral of the force acting on dA created by intravesical pressure is the support force acting on the magnetic mover from urinary bladder.

$$R = \int \mathrm{d}R = \int p \mathrm{d}A = pA_{\mathrm{R}} \tag{26}$$

where, p denotes intravesical pressure; A_{R} represents the projective area of the contact surface in the support force direction.

From Eq. (21), and Eq. (23) to Eq. (26), we can educe the intravesical pressure of urinary bladder.

$$p = K \frac{B_{\mathrm{r}} VNI}{\mu_{\mathrm{rec}} A_{\mathrm{R}}} \frac{\sum_{i=1}^{n} \frac{1}{\delta_i^2} (1 + \chi \tan\theta_i) \left[\sin\theta_i \sin(\alpha+\beta) + \sin\alpha - \sin\beta \right]}{\cos\gamma(\sin\alpha - \sin\beta) - \sin\gamma(\cos\alpha + \cos\beta)} \tag{27}$$

Considering the structure in Fig. 2, we let $\alpha \approx 90°$, $\beta \approx 0°$. Therefore, the intravesical pressure can be simplified as

$$p = K \frac{B_{\mathrm{r}} VNI}{\mu_{\mathrm{rec}} A_{\mathrm{R}}} \frac{\sum_{i=1}^{n} \frac{1}{\delta_i^2} (1 + \chi \tan\theta_i)(1 + \sin\theta_i)}{\cos\gamma - \sin\gamma} \tag{28}$$

The urine flow in urethra can be regarded as laminar flow. So, the urine flow rate in urethra can be expressed as

$$q = \frac{\pi d^4}{128 \mu l} p \tag{29}$$

where, d is the equivalent inner diameter of urethra; μ is the dynamic viscosity of urine; l is the length of urethra.

By substituting Eq. (28) into Eq. (29), the urine flow rate can be gained

$$q = K \frac{\pi d^4}{128 \mu l} \frac{B_{\mathrm{r}} VNI}{\mu_{\mathrm{rec}} A_{\mathrm{R}}} \frac{\sum_{i=1}^{n} \frac{1}{\delta_i^2} (1 + \chi \tan\theta_i)(1 + \sin\theta_i)}{\cos\gamma - \sin\gamma} \tag{30}$$

Equations (28) and (30) express the intravesical pressure and urine flow rate performance of the BPP, which is called the micturition performance of the BPP in this study. It is thus clear that the micturition performance is mainly affected by control parameter, electromagnet exciting current, and structure parameters, such as the turns of coil, the number, volume of PM, and so on. After the structure parameters are determined, the intravesical pressure and urine flow rate can be controlled by adjusting electromagnet exciting current.

4. SIMULATED EXPERIMENT SYSTEM

4.1 Design of Simulated Experimental System

In order to analyze and investigate the working principle and micturition performance of the BPP, a simulated experiment system was designed in this study according to the similarity criterion of fluid dynamincs [19].

As shown in Fig. 7, the system contains simulated urinary unit and measure-control unit. The simulated urinary unit is composed of magnetic mover, water bag, inlet pipe, upper water cup, drainage pipe, lower water cup, amplifier, and external electromagnet. It is used for simulating the function and urine fluid environment

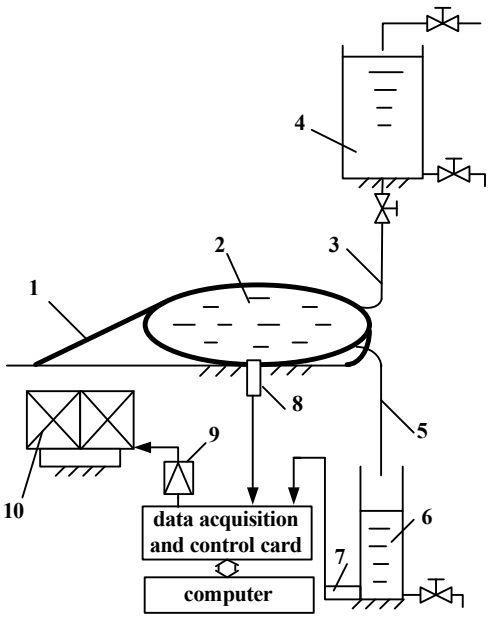


Fig. 7 Scheme map of simulated experiment system: 1. magnetic mover; 2. water bag; 3. inlet pipe; 4.upper water cup; 5. drainage pipe; 6. lower water cup; 7,8. pressure sensor; 9. amplifier; 10. external electromagnet

https://doi.org/10.1017/jmech.2012.106 Published online by Cambridge University Press

of the human urinary system that is composed of kidney, ureters, urinary bladder and urethra. The water bag, inlet, and drainage pipes are bladder physical model, ureter physical model, and urethra physical model respectively. The measure-control unit consists of computer, data acquisition and control card, pressure sensors. It is used for monitoring urodynamic parameteres and generating control signal to the amplifier.

In order to simulate the urine fluid environment of human urinary system accurately, the simulated urinary unit should have the similarity with human urinary system. Therefore, the simulated urinary unit was designed in this study according to the similarity criterion of fluid dynamics. Here, human urinary system and simulated urinary unit are respectively called prototype and model.

In the design of the model, it is assumed that the density and viscosity of the liquid in prototype are equal to the ones in model, the roughness of the object contacting with the liquid in prototype is the same as the one in model, the liquids in both prototype and model are incompressible, and the gravities of liquids in both prototype and model are neglected.

In this study, the design of the model is to educe the scale ratios of all relevant variables according to the appropriate similarity criterion [20].

Since viscous force acts on the liquid, similarity condition should meet Reynolds similarity criterion

$$(R_e)_p = (R_e)_m \tag{31}$$

i.e.

$$\frac{V_p l_p}{v_p} = \frac{V_m l_m}{v_m} \tag{32}$$

where, $(R_e)_p$ and $(R_e)_m$ are the Reynolds numbers of prototype and model respectively; V_p and V_m are the flow velocities of prototype and model respectively; v_p and v_m are the kinematic viscosities of prototype and model respectively; l_p and l_m are the lengths of prototype and model respectively.

Equation (32) becomes

$$\frac{V_p}{V_m} = \frac{v_p}{v_m}\frac{l_m}{l_p} \tag{33}$$

Equation (33) is written as

$$\lambda_V = \lambda_v \lambda_l^{-1} \tag{34}$$

where, λ_V is the scale ratio of flow velocity; λ_v is the scale ratio of kinematic viscosity; λ_l is the scale ratio of length.

Since the flow of liquid is caused by pressure drop, similarity condition should meet Euler similarity criterion

$$(E_u)_p = (E_u)_m \tag{35}$$

i.e.

$$\frac{p_p}{\rho_p V_p^2} = \frac{p_m}{\rho_m V_m^2} \tag{36}$$

where, $(E_u)_p$ and $(E_u)_m$ are the Euler numbers of prototype and model respectively; p_p and p_m are the pressures of prototype and model respectively; ρ_p and ρ_m are the densities of prototype and model respectively.

Equation (36) can be written as

$$\lambda_p = \lambda_\rho \lambda_V^2 \tag{37}$$

where, λ_p is the scale ratio of pressure; λ_ρ is the scale ratio of density.

By taking the assumptions $\lambda_v = 1$ and $\lambda_\rho = 1$ into Eqs. (34) and (37), and using the correspond equations, the scale ratio of each relevant variable can be educed.

The scale ratios in this study are shown in Table 1. After the scale ratio of length is determined, the other scale ratios can be obtained from Table 1.

Table 1 Scale ratios

Variable	Scale ratios	Equation
scale ratio of flow velocity λ_V	λ_l^{-1}	$\lambda_V = \lambda_v \lambda_l^{-1}$
scale ratio of time λ_t	λ_l^2	$\lambda_t = \lambda_l / \lambda_V$
scale ratio of flow λ_Q	λ_l	$\lambda_Q = \lambda_V \lambda_l^2$
scale ratio of acceleration λ_a	λ_l^{-3}	$\lambda_a = \lambda_V / \lambda_t$
scale ratio of pressure λ_p	λ_l^{-2}	$\lambda_p = \lambda_\rho \lambda_V^2$

4.2 Measuring Method of Urodynamic Parameteres

Some of the main urodynamic parameteres, such as intravesical pressure, urine flow rate, is usually measured in hospital to evaluate the functions of transportation, storage and micturition of urinary system. So, in this study, we need measure the water pressure in water bag and the flow rate in drainage pipe in order to evaluate the effectiveness of the BPP.

In simulated experiment system, the pressure sensor 8 is used for detecting the water pressure in water bag, indicating the intravesical pressure of bladder physical model. The pressure sensor 9 is used for measuring the water pressure in lower water cup, indirectly indicating the urine flow rate in urethra physical model.

Since urine flow rate can be expressed as

$$q = \frac{\Delta V_c}{\Delta t} = \frac{A}{\rho g}\frac{\Delta p_c}{\Delta t} \tag{38}$$

where, V_c is the water volume of lower water cup; p_c is the water pressure of lower water cup; A is the cross section area of lower water cup; ρ is the density of water; g is the acceleration of gravity.

It is seen that the urine flow rate can be gained by measuring the change rate of the water pressure in lower water cup.

5. SIMULATION AND EXPERIMENT

In order to validate the established mathematic models and investigate the micturition performance of the

https://doi.org/10.1017/jmech.2012.106 Published online by Cambridge University Press

BPP, we performed a great deal of simulation and experiment researches in this study. The simulation research was conducted by using ANSYS and MATLAB software. The experiment research was carried out in a simulated experiment apparatus. As shown in Fig. 8, it is developed under $\lambda_l = 1$, according to the above design scheme of simulated experiment system.

The main parameters of the BPP used for simulation and experiment are shown in Table 2.

In previous study, we had computed the electromagnetic driving force using ANSYS software and the established 3-D finite element model (3-D FEM) [21]. The computation results showed that the 3-D FEM is accurate and credible. In this study, we compared the electromagnetic driving force computed by the 3-D FEM with that determined by the above mathematic model (MM) under various parameters. By assuming that the electromagnetic driving forces gained by both models are approximately equal under same parameters, the flux leakage coefficient is finally determined as $K = 0.3$.

Figure 9 shows the simulation and experimental curves of the relationship between elctromagnetic driving force and electromagnet exciting current. In simulation and experiment, the number and initial angle of PMs are respectively: n = 2 and $\theta = 30°$. It can be seen from Fig. 9 that the elctromagnetic driving force augments proportionally with the increase of electromagnet exciting current.

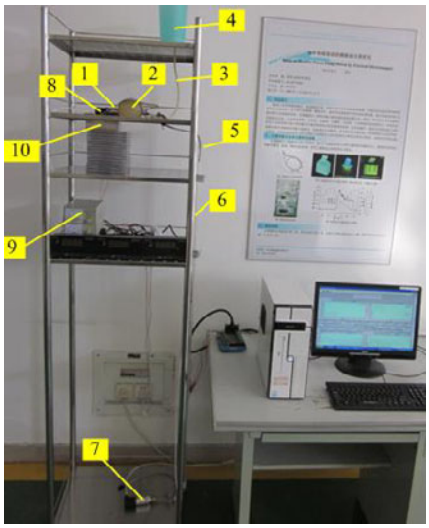


Fig. 8 Simulated experiment apparatus:1.magnetic mover; 2.bladder physical model; 3.ureter physical model; 4.water cup; 5.urethra physical model; 6.measuring cup; 7,8.pressure sensor; 9.amplifier; 10.external electromagnet

Table 2 Main parameters of BPP.

Structure	Parameters
electromagnetic drive	$V = 50\times25\times4\text{mm}^3$; $B_r = 1.17$T; $\mu_{rec} = 1.1$;$\mu = 1.0\times10^{-3}$Pa·s $\theta = 30°$; $N = 920$; $K = 0.3$; interval of PMs = 8mm; distance from electromagnet to stator = 20mm
urethra physical model	$d = 2.5$mm; $l = 200$m

Figure 10 shows the simulation and experimental curves of the relationship between elctromagnetic driving force and initial angle of PMs. In simulation and experiment, the number of PMs and electromagnet exciting current are respectively: n = 2 and $I = 3$A. From Fig. 10, it can be seen that the elctromagnetic driving force increases with the decrease of the initial angle of PMs. It implies that the PMs can be drawn onto the stator one by one, and the magnetic mover is capable of pressing urinary bladder micturating continuously.

In order to investigate the capability of establishing intravesical pressure using electromagnetic drive instead of urinary bladder detrusor in the urine storage stage, we examined the change of intravesical pressure, in simulation and experiment, by adjusting the electromagnet exciting current. Figure 11 shows the simulation and experimental curves of the relationship between intravesical pressure and electromagnet exciting current. It is seen that the intravesical pressure can augment proportionally with the increase of electromagnet exciting current.

In order to investigate the capability of establishing maximal urine flow rate using electromagnetic drive instead of urinary bladder detrusor in the micturition stage, we also examined the change of maximal urine flow rate, in simulation and experiment, by adjusting the electromagnet exciting current. Figure 12 shows the simulation and experimental curves of the relationship between maximal urine flow rate and electromagnet exciting current. It is also found that the maximal urine flow rate can increase proportionally with the increase of electromagnet exciting current.

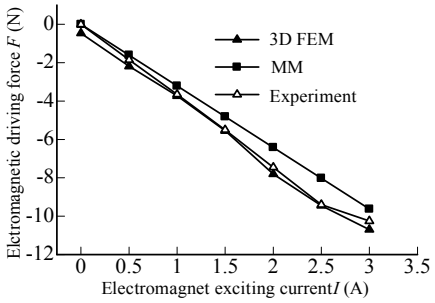


Fig. 9 Simulation and experimental curves of relationship between elctromagnetic driving force and electromagnet exciting current

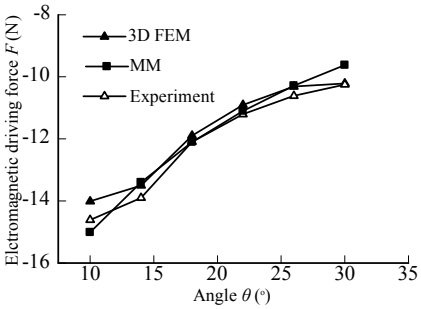


Fig. 10 Simulation and experimental curves of relationship between elctromagnetic driving force and initial angle of PMs

https://doi.org/10.1017/jmech.2012.106 Published online by Cambridge University Press

From Figs. 9 to 12, it can be seen that the simulation results of mathematic models basically accorded with the experimental results.

Figures 13(a) and 13(b) show the experimental curves of the intravesical pressure and urine flow rate of bladder physical model in the urine storage and micturition stages. In experiment, the number of PMs and electromagnet exciting current are respectively: n = 2 and I = 2A. It is seen from Figs. 13(a) and 13(b) that the established intravesical pressure in the urine storage stage can arrive at 3.2KPa, and maximal urine flow rate in the micturition stage reaches at 13.3cm^3/s. In generally, for a normal people whose voided volume is in 150-450cm^3, the maximal urine flow rate is more than 15cm^3/s, and the intravesical pressure is less than 12KPa [1]. Thus, it means that the micturition performance of the BPP approaches to that of human urinary bladder detrusor.

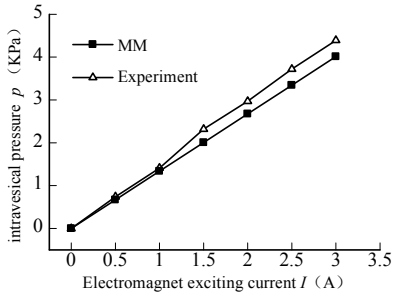


Fig. 11 Simulation and experimental curves of relationship between intravesical pressure and electromagnet exciting current

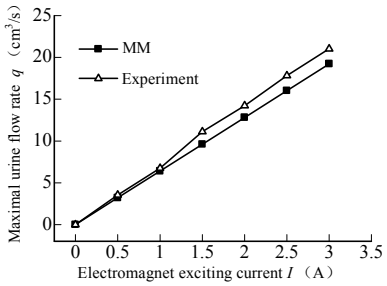


Fig. 12 Simulation and experimental curves of the relationship between maximal urine flow rate and electromagnet exciting current

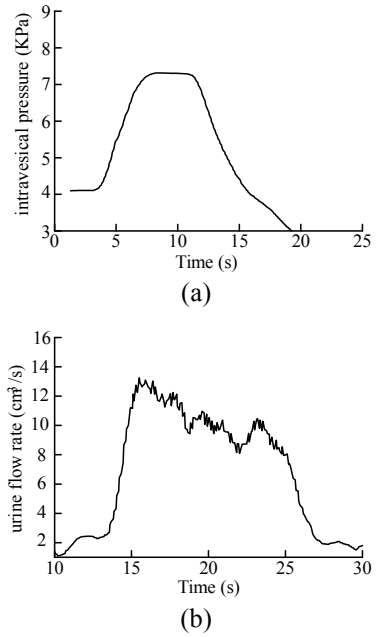


Fig. 13 Experimental curves of intravesical pressure and urine flow rate of bladder physical model, (a) intravesical pressure, (b) urine flow rate

CONCLUSIONS

The intravesical pressure and urine flow rate of the BPP can be controlled by adjusting electromagnet exciting current. The working principle of the BPP is feasible.

The established mathematic models are simple, practicable, and thus can provide the theoretical guidance for the performance analysis and structural optimazation design of the BPP.

The micturition performance of the BPP is basically accordant with that of human urinary bladder detrusor. But, the structure and parameters need be improved and optimized in order to obtain the optimal working performance of the BPP.

ACKNOWLEDGMENTS

This research is supported by Natural Science Foundation of China (Grant no. 50775040) and Guangdong Provincial Natural Science Foundation of China (Grant no. 07001746). The authors' special thanks go to our colleagues, associate Prof. Yinhui Ao, Dr. Zhijun Yang, and Mr. Dongcai Zhou for their contributions to the research program.

REFERENCES

1. Chen, Z., Chui, Z. and Shuang, W. B., *Neurogenic Bladder*, People's Medical Publishing House, Beijing, China (2009).
2. Frenkl, T. L. and Rackley, R. R., "Injectable Neuromodulatory Agents: Botulinum Toxin Therapy," *Urologic Clinics of North America*, **1**, pp. 89–99 (2005).
3. Oerlemans, D. J. and van Kerrebroeck, P. E., "Sacral Nerve Stimulation for Neuromodulation of the Lower Urinary Tract," *Neurourol Urodyn.*, **1**, pp. 28–33 (2008).
4. Vaidyananthan, S., Soni, B. M. and Brown, E., "Effect of Intermittent Urethral Catheterization and Oxybutynin Bladder Instillation on Urinary Continence Status and Quality of Life in a Selected Group of Spinal Cord Injury Patients with Neuropathic

https://doi.org/10.1017/jmech.2012.106 Published online by Cambridge University Press

Bladder Dysfunction," *Spinal Cord.*, **6**, pp. 409–414 (1998).
5. Wein, A. J., "The Ice-Water Test in the Diagnosis and Treatment of the Neurogenic Bladder," *Journal of Urology*, **6**, p. 2266 (1998).
6. Winn, C. and Thompson, J., "Urinary Catheters for Intermittent Use," *Journal of Professional Nursing*, **8**, pp. 541–548 (1998).
7. Fowler, C. J., Beck, R. O., Gerrard, S., Betts, C. D. and Fowler, C. G., "Intravesical Capsaicin for Treatment of Detrusor Hyperreflexia," *Journal of Neurology, Neurosurgery and Psychiatry*, **57**, pp. 169–173 (1994).
8. Lazzeri, M., Spinelli, M., Zanollo, A. and Turini, D., "Intravesical Vanilloids and Neurogenic Incontinence: Ten Years Experience," *Urologia Internationalis*, **2**, pp. 145–149 (2004).
9. Wiart, L., Joseph, P. A., Petit, H., Dosque, J. P., de Sèze, M., Brochet, B., Deminière, C., Ferrière, J. M., Mazaux, J.M., N'Guyen, P. and Barat, M., "The Effects of Capsaicin on the Neurogenic Hyperreflexic Detrusor. A Double Blind Placebo Controlled Study in Patient with Spinal Cord Disease. Preliminary Results," *Spinal Cord*, **36**, pp. 95–99 (1998).
10. Robin, S., Sawan, M., Abdel-Gawad, M., Abdel-Baky, T. M. and Elhilali, M. M., "Implantable Stimulation System Dedicated for Neural Selective Stimulation," *Medical and Biological Engineering and Computing*, **36**, pp. 490–492 (1998).
11. Xiao, C. G. and Godec, C. J., "A Possible New Reflex Pathway for Micturition After Spinal Cord Injury," *Paraplegia*, **5**, pp. 300–307 (1994).
12. Xiao, C. G., Du, M. X., Dai, C., Li, B., Nitti, V. W. and de Groat, W. C., "An Artificial Somatic-Central Nervous System-Autonomic Reflex Pathway for Controllable Micturition After Spinal Cord Injury: Preliminary Results in 15 Patients," *Journal of Urology*, **170**, pp. 1237–1241 (2003).
13. Li, S. L., Chen, W. X., Chen, Y. L., Li, J. L., Lin, P. and Sun, D. Q., "Surgical Procedures of Neurogenic Bladder and Analysis of the Complications," *Chinese Journal of Urology*, **7**, pp. 464–467 (2005).
14. Kazuo, K., Yoshihiko, S., Jiro, U. and Keiji, N., "A Study on Implantable Urination Assist Systems - Development of a Bladder Compression System," *Proceedings of the 26th Annual International Conference of the IEEE EMBS*, San Francisco, CA USA, pp. 2774–2776 (2004).
15. Kiguchi, K., Sakamoto, Y. and Nakashima, K., "Development of an Urination Assist System - A Bladder Compressing System with a Link-Work Mechanism," *Proceedings of 2007 IEEE International Conference of Mechatronics*, pp. 526–531 (2007).
16. Xiao, L. and Ting, G., "A Bladder Power Pump Driven by External Electromagnet," *China Patent*, ZL200710031081.1 (2010).
17. Min, Z. L., *Chinese Urology*, People's Military Medical Press, Beijing, China (2003).
18. Chen, Z. and Cui, Z. Q., *Fundamentals of Electromagnetics Theory*, Beijing Institute of Technology Press, Beijing, China (2002).
19. Xiao, L. and Ting, G., "Design of Bladder Power Pump Driven by External Electromagnet and Simulated Experimental System," *Machine Tool and Hydraulics*, **11**, pp. 71–73 (2009).
20. Li, Y. Z. and Yuan, M. S., *Fluid Dynamics*, Higher Education Press, Beijing, China (2008).
21. Xiao, L., Weijia, H. and Ting, G., "FEM Analysis of Electromagnetic Drive of Bladder Power Pump," *Proceedings of the 4th International Conference on Bioinformatics and Biomedical Engineering*, Chengdu, China, **2**, 5515370 (2010).

(Manuscript received September 22, 2011, accepted for publication March 30, 2012.)

https://doi.org/10.1017/jmech.2012.106 Published online by Cambridge University Press